

Forced Oscillation Identification and Filtering from Multi-Channel Time-Frequency Representation

Pablo Gill Estevez, Pablo Marchi, Francisco Messina, and Cecilia Galarza

Abstract—Location of non-stationary forced oscillation (FO) sources can be a challenging task, especially in cases under resonance condition with natural system modes, where the magnitudes of the oscillations could be greater in places far from the source. Therefore, it is of interest to construct a global time-frequency (TF) representation (TFR) of the system, which can capture the oscillatory components present in the system. In this paper we develop a systematic methodology for frequency identification and component filtering of non-stationary power system forced oscillations (FO) based on multi-channel TFR. The frequencies of the oscillatory components are identified on the TF plane by applying a modified ridge estimation algorithm. Then, filtering of the components is carried out on the TF plane applying the anti-transform functions over the individual TFRs around the identified ridges. This step constitutes an initial stage for the application of the Dissipating Energy Flow (DEF) method used to locate FO sources. Besides, we compare three TF approaches: short-time Fourier transform (STFT), STFT-based synchrosqueezing transform (FSST) and second order FSST (FSST2). Simulated signals and signals from real operation are used show that the proposed method provides a systematic framework for identification and filtering of power systems non-stationary forced oscillations.

Index Terms—Forced oscillations, phasor measurement unit (PMU), time-frequency analysis, synchrosqueezing, multicomponent signals, non-stationary signal.

I. INTRODUCTION

FORCED oscillations (FOs) are determined by inputs and disturbances that drive the system, unlike modal oscillations which mainly depend on the dynamic characteristics of the system [1], [2]. FOs can occur in power systems due to different causes, such as equipment failure, inadequate control designs, and abnormal generator operating conditions [3]. The most efficient way for mitigating sustained oscillations is to locate the source and to disconnect it from the network [4]. Many methods for locating the source have been proposed in the past few years [5], among these methods, Dissipating Energy Flow (DEF) method [4] has shown a good performance for oscillation source location, and it was recently adopted by Independent System Operator - New England (ISO-NE) [6].

Fig. 1 shows active power flows through transmission line Sub2-Ln3 of the October 3, 2017 event in ISO-NE [7]. Non-sinusoidal and non-stationary nature of the oscillation can be identified. Non-stationary oscillating signal are typically represented as multicomponent signals (MCSs) by a superposition of amplitude- and frequency-modulated (AM-FM)

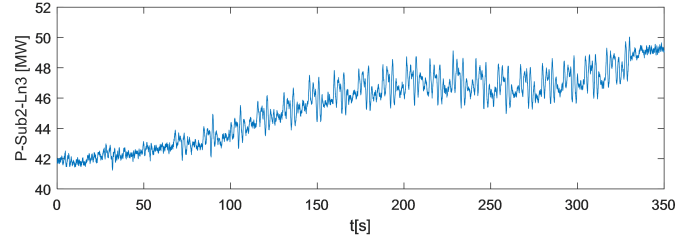


Fig. 1. Active Power Flow during October 3, 2017 event in ISO-NE [7].

components. Filtering and extracting the oscillatory components for forced oscillations is a commonly used step in methods for locating oscillation sources, such as DEF method [8]. Time-frequency (TF) analysis extracts the temporal and spectral information from the signal simultaneously, providing a suitable framework for studying non-stationary signals. The information of the different components of a MCS in the TF plane spreads around curves commonly called ridges. The short-time Fourier transform (STFT) is probably one of the best known TF analysis tools. On the other hand, a widely used tool for signal decomposition is the Synchrosqueezing Transform (SST) [9] that was originally introduced in the context of Continuous Wavelet Transform (CWT) [9] and then extended to STFT [10], referred as STFT-based SST (FSST). FSST reassigns the information of STFT, sharpening the representation in the TF plane, on which oscillatory components of the signal are identified and then extracted and transformed into the time domain. The applicability of SST is restricted to MCSs made of slightly modulated harmonic modes. In order to deal with stronger amplitude and frequency modulations, an extension based on linear chirp approximation called second-order STFT-based SST (FSST2) was introduced in [11] [12]. As an example, Fig. 2 shows STFT, FSST and FSST2 of the signal in Fig. 1. We can observe multiple regions with variable frequency and amplitude in the TF plane, centered around the ridges (in this case ridges represent signal harmonics). The details in the figure show how FSST improves the concentration around the ridges over STFT and, FSST2 improves it over FSST.

In particular, FSST was applied by the authors in [13] as TF approach for filtering signal components before the application of DEF method. In this case, the frequency identification was carried out locally in each generator or branch, without being able to take advantage of the simultaneity characteristics provided by the PMU measurements. Additionally, the ridge identification algorithm was only limited to cases where the oscillatory component was present in the entire analysis window, without considering the possibility that an oscillatory component of the signal may begin or disappear during the

P. Gill Estevez, P. Marchi, F. Messina, and C. G. Galarza work with the School of Engineering, Universidad de Buenos Aires and the CSC-CONICET, Argentina. (e-mail: pgill@fi.uba.ar, pmarchi@fi.uba.ar, fmessina@fi.uba.ar, cgalar@fi.uba.ar)

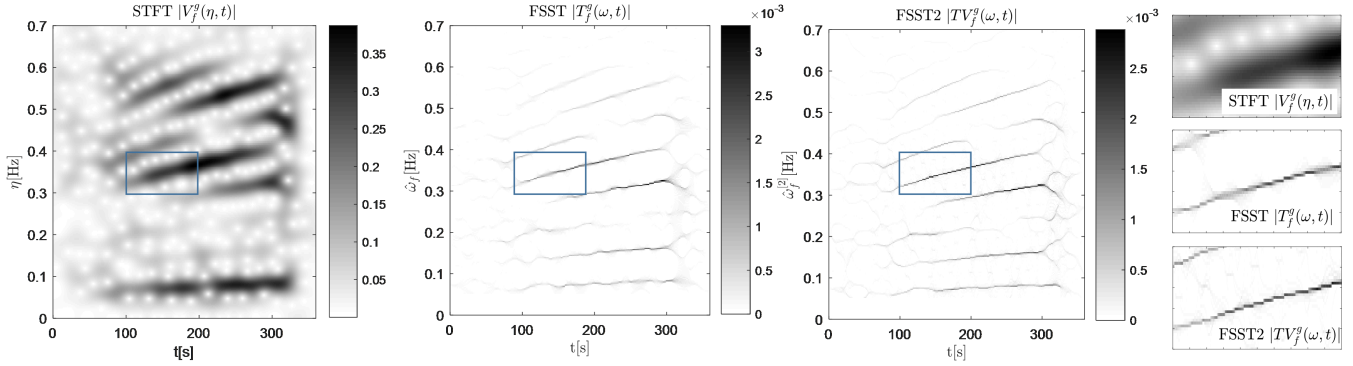


Fig. 2. STFT, FSST and FSST2 of active power flow P-Sub2-Ln3 during October 3, 2017 event in ISO-NE [7].

analysis window. The reconstruction of the signal components as a function of the inverse SST was done using a fixed frequency band.

The main goal of this paper is to develop a systematic methodology for identification and filtering from multi-channel TF representation to retrieve the oscillatory components of non-stationary power system forced oscillations. We introduce an improved ridge identification algorithm and an improved hard-thresholding reconstruction. Besides, we compare the performance of the method on simulated and real operation data using three different TF representations: STFT, FSST and FSST2.

II. MATHEMATICAL BACKGROUND

A. Multi-component Signal

Non-stationary oscillatory data $f(t)$ is represented by a MCS as a superposition of H oscillatory components as:

$$f(t) = \sum_{h=1}^H f_h(t) + r(t), \quad (1)$$

where each oscillatory component $f_h(t) = A_h(t)e^{j2\pi\phi_h(t)}$ has a time-varying amplitude $A_h(t)$ and instantaneous frequency (IF) $\phi'_h(t)$. The signal $r(t)$ represents noise plus low frequency trend signal [14]. We further assume that the modes are separated in frequency with resolution Δ : $\forall h \leq H-1, \phi'_{h+1}(t) - \phi'_h(t) > 2\Delta$. In the TF plane, the different components are associated with so-called ridges, which are denoted $(\phi'_h)_{h=1, \dots, H}$, that are estimates of the IFs $(\phi'_h)_{h=1, \dots, H}$ of the components.

B. Short-time Fourier transform (STFT)

We denote by \hat{f} the Fourier transform of function s with the following normalization:

$$\hat{f}(\eta) = \int_{\mathbb{R}} f(x)e^{-2j\pi\eta x} dx \quad (2)$$

The STFT is a local version of the Fourier transform obtained by means of a sliding window g [10]:

$$V_f^g(t, \eta) = \int_{\mathbb{R}} f(u)g(u-t)e^{-2j\pi\eta(u-t)} du \quad (3)$$

Considers that the signal \mathbf{f} is a discrete time sequence of length L such that $\mathbf{f}[n] = f(\frac{nT}{L})$, for $n = 0, \dots, L-1$, and that $(\mathbf{g}[n])_{n \in \mathbb{Z}}$ are the samples at $\frac{T}{L}$ of the Gaussian window, which is further truncated to be supported on $-M, \dots, M$ such that $2M+1 \leq N$, where N is the number of frequency bins. The sampling frequency is $F_s = L/T$. In that context, the discrete STFT of \mathbf{f} is defined by [15]

$$\mathbf{V}_f^g[m, k] = \frac{1}{N} \sum_{n \in \mathbb{Z}} \mathbf{f}[n]\mathbf{g}[n-m]e^{-2j\pi\frac{k(n-m)}{N}} \quad (4)$$

$$= \frac{1}{N} \sum_{n=-M}^M \mathbf{f}[m+n]\mathbf{g}[n]e^{-2j\pi\frac{kn}{N}} \quad (5)$$

with $k \in \{0, \dots, N-1\}$ and $m \in \{0, \dots, L-1\}$ which can be computed for each m through a discrete Fourier transform of length N . The index k corresponds to a frequency in $I_L = 0, \frac{L}{N}, \dots, (N-1)\frac{L}{N}$, and the index n to time $\frac{nT}{L}$. The reconstruction formula is

$$\mathbf{f}[m] = \frac{1}{g(0)} \sum_{k=0}^{N-1} \mathbf{V}_f^g[m, k] \quad (6)$$

If we assume slow variations in $A_h(t)$ and on the IF $\phi'_h(t)$ of a MCS, we can write the following approximation in the vicinity of a fixed time t_0 :

$$f(t) \approx \sum_{h=1}^H A_h(t_0)e^{j2\pi[\phi_h(t_0) + \phi'_h(t_0)(t-t_0)]} \quad (7)$$

The corresponding approximation for the STFT then results (changing t_0 by a generic t):

$$V_f^g(t, \eta) \approx \sum_{h=1}^H f_h(t)\hat{g}(\eta - \phi'_h(t)) \quad (8)$$

The representation of this multicomponent signal by $V_f^g(t, \eta)$ in the TF plane shows that the peaks are concentrated around ridges defined by $\eta = \phi'_h(t)$. The frequency width around each ridge is related to the frequency bandwidth of \hat{g} . Considering a gaussian window $g(t) = e^{-\pi t^2/\sigma^2}$, then the standard deviation is $std_g = \sigma/(\sqrt{2\pi})$ and the standard deviation of \hat{g} results $std_{\hat{g}} = 1/(\sqrt{2\pi}\sigma)$.

C. STFT-based synchrosqueezing transform

Starting from STFT, the FSST moves the coefficients $V_f^g(t, \eta)$ according to the map $(t, \eta) \mapsto (t, \hat{\omega}_f(t, \eta))$, where $\hat{\omega}_f(t, \eta)$ is the local instantaneous frequency defined as

$$\hat{\omega}_f(t, \eta) = \frac{1}{2\pi} \partial_t \arg(V_f^g(t, \eta)) = \eta + \text{Im} \left\{ \frac{V_f^{g'}(t, \eta)}{2\pi V_f^g(t, \eta)} \right\} \quad (9)$$

FSST coefficients are given by [10]:

$$T_f^g(t, \omega) = \frac{1}{g(0)} \int_0^\infty V_f^g(t, \eta) \delta[\omega - \hat{\omega}_f(t, \eta)] d\eta \quad (10)$$

where δ denotes the Dirac distribution.

Calculating the FSST with (10) sharpens the information relative to components in the TF plane around the ridges. Ridges $\varphi'_h(t)$ associated to the h th component are estimated with the application of a specific algorithm. Each component f_h can be recovered by integrating $T_f^g(f, t)$ around a small frequency band d around the curve of [10]:

$$f_h^{FSST}(t) = \int_{|\omega - \varphi'_h(t)| < d} T_f^g(t, \omega) d\omega \quad (11)$$

We define a discrete-time version of $T_f^g(t, \omega)$, denoted by $\mathbf{T}_f^g[m, k]$.

D. Second-order STFT-based synchrosqueezing transforms

FSST assumes $\phi''(t)$ is negligible but in many situations the signal exhibits high frequency modulation [12] and the applicability of FSST could be restricted. For this cases, an extension based on linear chirp approximation was introduced, called second-order STFT-based synchrosqueezing transform (FSST2) [11] [12]. It uses a more accurate IF estimate than $\hat{\omega}_f$, named as second-order instantaneous frequency estimator of f defined by [11]

$$\hat{\omega}_f^{[2]}(t, \eta) = \begin{cases} \hat{\omega}_f(t, \eta) + \hat{q}_f(\eta, t)(t - \hat{\tau}_f(t, \eta)) & \text{if } \partial_t \hat{\tau}_f(t, \eta) \neq 0 \\ \hat{\omega}_f(t, \eta) & \text{otherwise} \end{cases} \quad (12)$$

Where the modulation operator $\hat{q}_f(\eta, t)$ is computed by [11]:

$$\hat{q}_f(\eta, t) = \text{Re} \left\{ \frac{1}{2i\pi} \frac{V_f^{g''} V_f^g - (V_f^{g'})^2}{(V_f^g)^2 + V_f^{tg} V_f^{g'} - V_f^{tg'} V_f^g} \right\} \quad (13)$$

To enlighten the notation we write V_f^g instead of $V_f^g(t, \eta)$. If $h(t) = A(t)e^{2i\pi\phi(t)}$ is a linear chirp with $\phi(t)$ and $\log(A(t))$ quadratic functions, then $\hat{q}_h = \phi''$ and $\hat{\omega}_h^{[2]}(t, \eta) = \phi'(t)$ [16]. FSST2 is defined by

$$TV_f^g(t, \omega) = \frac{1}{g(0)} \int_0^\infty V_f^g(t, \eta) \delta[\omega - \hat{\omega}_f^{[2]}(t, \eta)] d\eta \quad (14)$$

A procedure analogous to that used with FSST can be used for ridge identification and component reconstruction from FSST2:

$$f_h^{FSST2}(t) = \int_{|\omega - \varphi'_h(t)| < d} TV_f^g(t, \omega) d\omega \quad (15)$$

Its discrete-time counterpart is denoted by $\mathbf{TV}_f^g[m, k]$.

E. Dissipating Energy Flow Method

The first steps of the DEF method are [8]:

- *PMU data pre-processing*. PMU angles for voltages and currents should be unwrapped. Replace missing PMU data (NaN) and outliers with interpolated data.
- *Frequency identification* of the sustained oscillation.
- *Filtering the component of interest* around the identified frequency applied to the variables of interest for DEF calculation (i.e. active and reactive power, voltage magnitude, angle, and frequency).

Then, the flow of dissipating transient energy is calculated in the branches of the systems for the filtered components. The rate of change of the dissipating energy flow allows tracing the source of sustained oscillations. The flow of dissipating energy, for specific filtered components in a branch ij from bus i , is expressed by integrating over the system trajectory as follows [8]:

$$W_h^{ij} \approx \int P_h^{ij} d\theta_h^i + \int Q_h^{ij} \frac{dv_h^i}{v^i}, \quad (16)$$

where P^i and Q^i are the active and reactive power flows in branch i , θ^i is the bus voltage angle, and v^i is the bus voltage magnitude. Subindex h indicates that the filtered magnitudes corresponding to h oscillatory component. The value and sign of the rate of change of W_h^{ij} have a physical interpretation as the amount and direction of the dissipating energy flow. It indicates the direction of the source location relative to the branch ij . Positive rate of change of W_h^{ij} means the source is located behind bus i , and a negative value means the source is located behind bus j or branch ij is the source [6]. For discrete PMU signals, a discrete-time approximation has the form:

$$W_h^{ij}[m] = W_h^{ij}[m-1] + P_h^{ij}[m-1] (\theta_h^i[m] - \theta_h^i[m-1]) + \frac{Q_h^{ij}[m-1]}{v^i[m-1]} (v_h^i[m] - v_h^i[m-1]) \quad (17)$$

where m represents the time instant. The integration limits are determined from the transient when sustained oscillations have significant magnitude larger than noise.

III. PROPOSED METHODOLOGY

Fig. 3 shows the scheme of proposed methodology. The methodology could be applied to any invertible TF representation. $TF_f(t, \omega)$ and $\mathbf{TF}_f[m, k]$ are used to generically name the coefficients for the continuous and the discrete time version of the TF representations of signal f .

A. Multi-channel TF representation

It is assumed that PMU measurements are available from B branches at different locations in the system. In order to capture the relevant oscillatory components for DEF calculation, we define a global TF representation of the system:

$$\mathbf{MTF}[m, k] = \sqrt{\sum_{i=1}^B |\mathbf{TF}_{P_i}[m, k]|^2 + |\mathbf{TF}_{Q_i}[m, k]|^2} \quad (18)$$

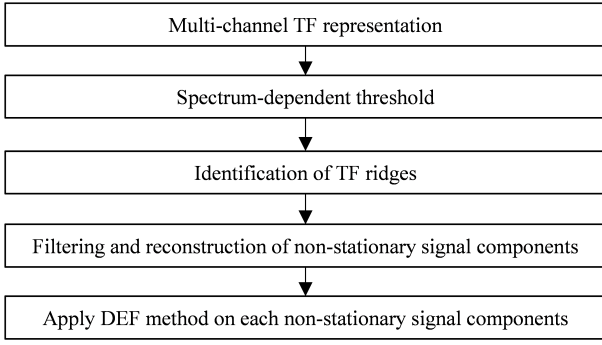


Fig. 3. Scheme of proposed methodology

where P^i and Q^i are the measurements of the active power flows and the reactive power flows of branches $i = 1, \dots, B$. P^i presents good observability for components of the electromechanical range, and is not as influenced by frequencies lower than 0.1 Hz as is the bus voltage angle [8]. Q^i allows to identify components in the upper part of the electromechanical range, which could be less observable in P^i .

B. Spectrum-Dependent Threshold

From measurements prior to the appearance of FO, a spectrum-dependent threshold $\gamma_M[k]$ for the multi-channel TF representation is defined, such that if $|\mathbf{MTF}[m, k]| < \gamma_M[k]$ then only ambient noise is considered present. For this, we calculate the value of $|\mathbf{MTF}[m, k]|$ that is not exceeded a certain percentage level of occurrence within a sliding rectangular window around each point of the TF plane, denoted as $\beta_M[m, k]$. In this work we use a sliding window of dimensions 0.1 Hz and 25 seconds centered at each point, and a level of 97%. The threshold is then defined by $\gamma_M(k) = \min_{m \in T_{pre}} \beta_M[m, k]$, where T_{pre} is the time lapse prior to the appearance of FO. Window overlapping makes the threshold variation with frequency smooth. Similarly, thresholds are defined for each of the signals, which will then be used in the filtering process. For example, $\gamma_{P^i}[k]$ is the threshold for active power flow of branch i , calculated from $|\mathbf{TF}_{P^i}[m, k]|$.

C. Ridge Estimation

In order to find the dominant ridges, the following optimization problem should be solved

$$\max_C \sum_{h=1}^H \int_{\mathbb{R}} |\mathbf{MTF}(t, \varphi_h(t))|^2 dt \quad (19)$$

where $C = \{\varphi_1(t), \dots, \varphi_H(t)\}$ is the set of estimated ridges. We use algorithm 1 to compute an estimate of the first H ridges with higher energy for a TF representation $\mathbf{MTF}[m, k]$, and the resulting ridges are identified in discrete time index $\varphi_1[m], \dots, \varphi_H[m]$. Algorithm 1 is a modified version of the algorithm in [17], the difference is that the search in the TF plane is performed in jumps instead of searching between contiguous time steps, allowing better performance in high-noise conditions. In addition, a frequency-dependent threshold is used, which improves the performance of the algorithm in power systems applications where the ambient

noise is colored. For the estimation of one ridge curve, the algorithm identifies U candidate curves from different initial points (chosen as the maximum of \mathbf{TF}_f in U time intervals). From that point, the algorithm first sweeps the TF plane in a positive direction of time (forward iteration) looking for a local maximum within the region described in Fig. 4. The parameters that determine the triangular search area (A_q^+ and A_q^-) are $jump_t$ (maximum temporal jump), $jump_f$ (maximum frequency jump) and max_{der} , which is the maximum derivative of frequency to limit frequency modulation of identified curves. The search is carried out while $|\mathbf{MTF}|$ is greater than the threshold $\gamma_M[k]$ beyond which the component is assumed to vanish. Then it performs an analogous iteration from the initial point but in the negative direction of time (backward iteration). We use parameter $jump_t$ corresponding to 2 seconds, $jump_f$ corresponding to 0.03 Hz and max_{der} corresponding to 0.03 Hz/s.

Algorithm 1: Ridge Estimation Algorithm

```

for  $h=1:H$  do
  for  $u=1:U$  do
    1. Define time interval for initial point
        $I_u = [(u-1)L/U, uL/U]$ .
    2. Find
        $[q_0, c_u[q_0]] = \underset{m \in I_u, k \in [0, N/2-1]}{\operatorname{argmax}} |\mathbf{MTF}[m, k]|$ 
    3. Iterate forward in time from  $q = q_0$ 
       while  $|\mathbf{MTF}[q, c_u[q]]| > \gamma_M[c_u[q]] \ \& \ q \leq L$ 
       do
          $[q^*, c_u[q^*]] = \underset{[m, k] \in A_q^+}{\operatorname{argmax}} |\mathbf{MTF}[m, k]|$ 
         Linear interpolation of intermediate points
          $q = q^*$ 
    4. Iterate backward in time from  $q = q_0$ 
       while  $|\mathbf{MTF}[q, c_u[q]]| > \gamma_M[c_u[q]] \ \& \ q \geq 1$ 
       do
          $[q^*, c_u[q^*]] = \underset{[m, k] \in A_q^-}{\operatorname{argmax}} |\mathbf{MTF}[m, k]|$ 
         Linear interpolation of intermediate points
          $q = q^*$ 
    5. Calculate energy
        $E_{c_u} = \sum_q |\mathbf{MTF}[q, c_u[q]]|^2$ 
    6. Adopt the highest energy curve whose length is
       greater than  $L_c$ 
        $\varphi_h[m] = \underset{c_u / \text{length}(c_u) > L_c}{\operatorname{argmax}} E_{c_u}$ 
    7. Peel component
        $\mathbf{MTF} = \mathbf{MTF} \setminus \bigcup_m [\varphi_h[m] - d_1, \varphi_h[m] + d_1]$ 
  
```

The candidate curve with the highest energy is chosen whose length is greater than a certain duration of time L_c (for example, a minimum of 25 seconds is considered to avoid capturing components that represent damped natural oscillations). Then, the peeling action is carried out, setting the coefficients associated with it to zero, in order to continue applying the algorithm to identify others. Set subtraction operation is indicated with \setminus in algorithm 1. d_1 is the thickness used to peel the ridge associated with an identified mode.

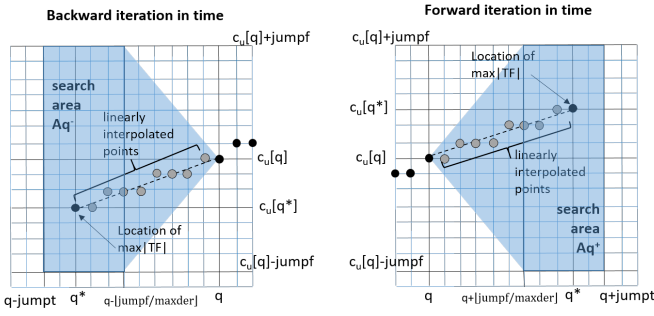


Fig. 4. Ridge identification algorithm search region

For STFT we choose $d_1 = \lceil 3std_{\hat{g}}N/Fs \rceil$, while for FSST or FSST2, due to the fact that the coefficients are more concentrated to the ridges, we use $d_1 = \lceil std_{\hat{g}}N/Fs \rceil$.

D. Filtering and reconstruction in time domain

Hard Thresholding (HT) technique, when used for retrieving the mode f_h of a MCS, considers in the reconstruction process only the coefficients of the TF representation in the vicinity of φ_h , whose magnitude is above a certain threshold [18] [15]. The frequency bands around each ridge used for mode reconstruction $J_{1,h}[m] = [\eta_{1,h}^-[m], \eta_{1,h}^+[m]]$ are

$$\eta_{1,h}^-[m] = \max \left\{ \eta_h^-[m], \varphi_h[m] - d_{max} \right\} \quad (20)$$

$$\eta_{1,h}^+[m] = \min \left\{ \eta_h^+[m], \varphi_h[m] + d_{max} \right\} \quad (21)$$

where

$$\eta_h^-[m] = \underset{k < \varphi_h[m] - d_{min}}{\operatorname{argmax}} \left\{ |\mathbf{TF}_f^g[m, k]| < \gamma_f[k] \right\} \quad (22)$$

$$\eta_h^+[m] = \underset{k > \varphi_h[m] + d_{min}}{\operatorname{argmin}} \left\{ |\mathbf{TF}_f^g[m, k]| < \gamma_f[k] \right\} \quad (23)$$

$\gamma_f[k]$ is frequency dependent threshold, d_{min} is the minimum band from which the threshold is checked and d_{max} is the maximum value for the band to avoid overlap of close modes and to establish a limit in low noise signals. The reconstruction in time domain then results (with $g(0) = 1$):

$$\mathbf{f}_h[m] = \sum_{k \in J_{1,h}[m]} \mathbf{TF}_f^g[m, k] \quad (24)$$

This reconstruction procedure can be applied to STFT, FSST and FSST2.

IV. NUMERICAL RESULTS

In this section, we present the analysis of two different examples applying STFT, FSST or FSST2. First, the proposed methodology is applied to simulated data obtained from the WECC179 model. Secondly, the proposed methodology is applied to real PMU measurements obtained from an event occurred in ISO-NE [7]. The code for the application of STFT, FSST, FSST2 is a modified version of [19]. The choice of parameter σ of the window is done by considering the minimal Rényi entropy of the FSST spectrum [13]. Since the frequency band of electromechanical phenomena in power systems is usually between 0.1 Hz and 2.5 Hz, a parameter σ that gives

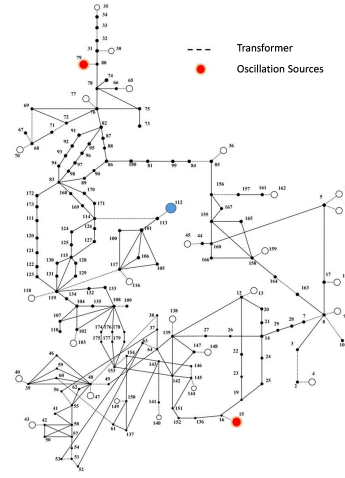


Fig. 5. WECC 179 bus system. Model data is obtained from [7]

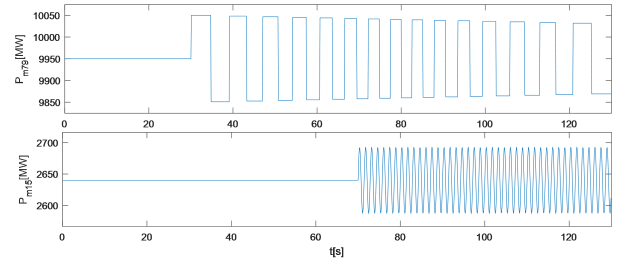


Fig. 6. Mechanical power of generator 79 and generator 15 (sources)

good results for different circumstances is the corresponding to std_g in the range from 2s to 10s. Once defined, the value of $\Delta = 3std_g$ is an indication to verify the condition of well separated modes in frequency.

A. WECC 179 bus

The described methodologies for the identification of oscillatory components are applied to simulated data from the WECC 179 model, whose one-line diagram is shown in Fig. 5. A non-stationary mechanical power is applied in generator 79 using a square signal whose fundamental frequency is linearly increased from 0.1 Hz to 0.2 Hz from $t = 30$ s to $t = 80$ s, and then linearly reduced to 0.1 Hz in other 50 seconds. This non-sinusoidal input with variable frequency produces a series of variable frequency harmonics that could interact with system natural modes at multiple frequencies. Additionally, a constant frequency disturbance of 0.7 Hz is added to the mechanical power of generator 15 at $t = 70$ s (shown in Fig. 6). White Gaussian noise was introduced in the loads during the simulation in order to generate colored ambient noise in the system magnitudes. Additive white noise with different levels was also added to the simulation results in order to evaluate the noise tolerance of the proposed algorithms.

1) *Frequency Identification*: We denote by $\alpha(t)$ an additive white Gaussian noise with zero mean and variance σ_α^2 , which is added to the simulated signals. The Signal-to-Noise Ratio (SNR) in dB will be defined by

$$SNR_{in}[dB] = 10 \log_{10}(Var(f)/\sigma_\alpha^2) \quad (25)$$

where $Var(f)$ is the variance of the noiseless signal f that contains the FO, resulting from simulation. Fig. 7 graphically

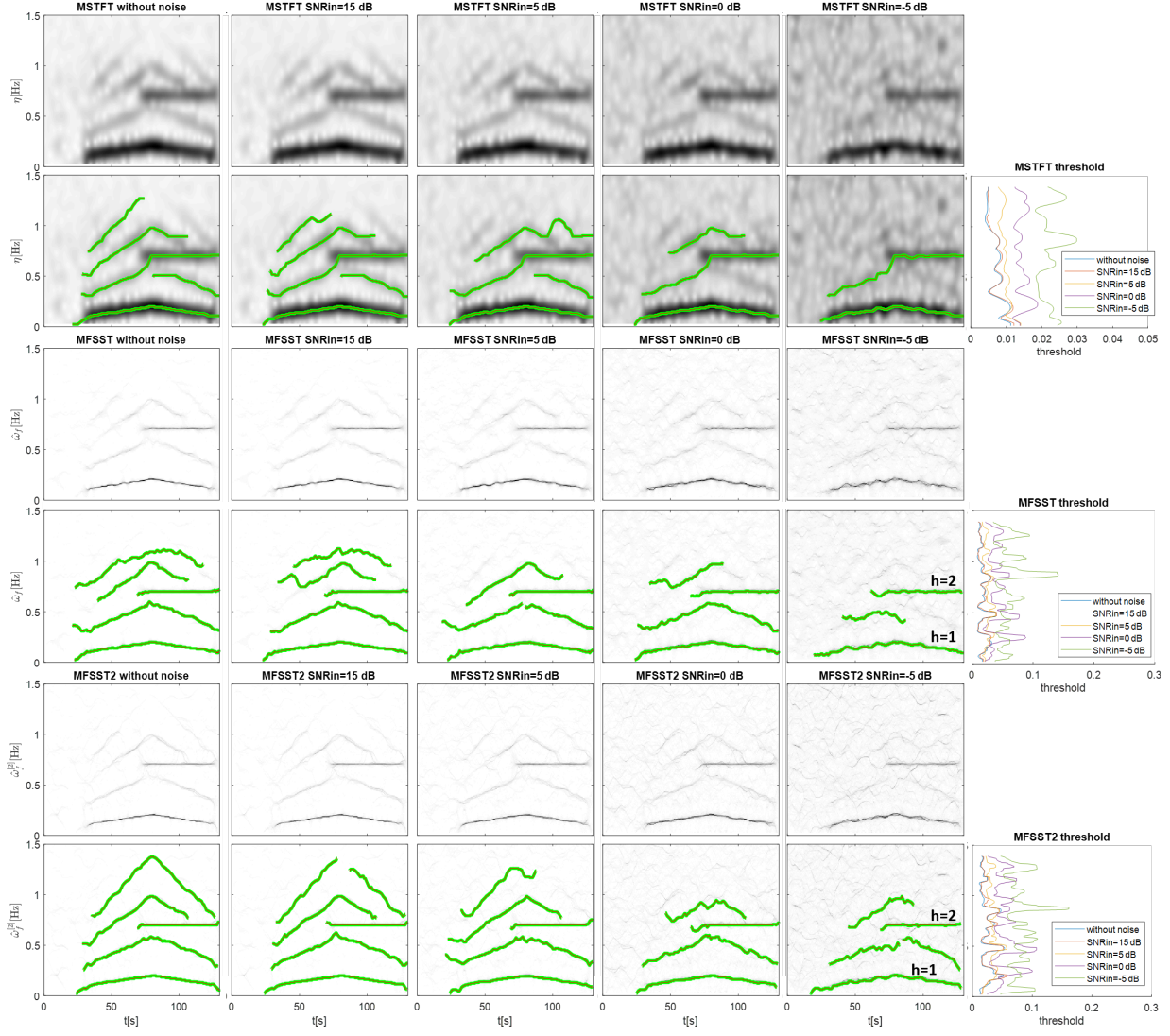


Fig. 7. Comparison of the application of algorithm 1 for frequency identification on multi-channel TFR based on STFT, FSST and FSST2, with different levels of additive noise. Identified ridges are shown as green curves in respective plots.

shows the results of the application of the multi-channel methodology using active and reactive power of all the generator in the system with three TF representations (STFT, FSST and FSST2), and different levels of additive noise. Algorithms are applied to identify a maximum of 7 components in each case, but the identified curves whose length is less than $L_c = 40$ seconds are discarded. The ridges resulting from the identification algorithm are shown in green. A pattern of time-varying components is observed. Even for low additive noise levels, ridge identification on STFT presents mode mixing problems, where the ridges includes the constant frequency component of 0.7Hz together with the third harmonic of square signal. FSST and FSST2 significantly reduce mode mixing problems because the spectrum is much more concentrated. In the case of FSST, it is not possible to identify the higher order harmonics due to their higher frequency modulation, even at low levels of added noise, unlike FSST2 where it is possible to identify the harmonics with the highest frequency modulation. In both (FSST and FSST2), as the additive noise increases, the lower amplitude harmonics are lost. However, even for an SNR

of -5dB, it is possible to identify the fundamental frequencies of both sources of oscillation with both FSST and FSST2.

2) *Filtering*: In order to compare the reconstruction error of each method, we define a root mean squared error by

$$RMSE = \frac{\|\hat{f} - f\|_2}{\|f\|_2} \quad (26)$$

where f is the signal without noise and \hat{f} is the reconstructed signal with a specific method, as the sum of the filtered components of each case. First, we analyze the impact of the value of the reconstruction band d_{min} for the FSST and FSST2 methods. Fig. 8 shows $RMSE$ calculated with the sum of the components $h = 1$ and $h = 2$, and taking as a reference the sum of the components $h = 1$ and $h = 2$ of the case without additive noise. $RMSE$ is represented as a function of d_{min} and SNR_{in} , and each point is calculated as the average value of 10 realizations of additive noise. In these tests we use an upper limit d_{max} corresponding to $3std_{\hat{g}}$, which is never reached because the FSST and FSST2 spectrum are highly concentrated in the ridges curves. For low noise levels,

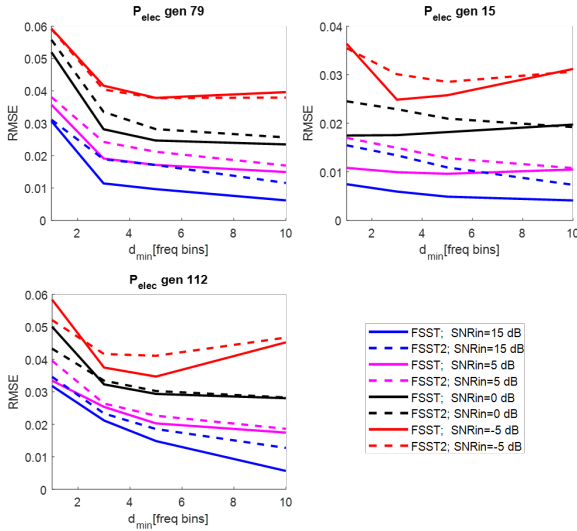


Fig. 8. Root mean squared error $RMSE$ of fundamental frequency components in electric power for different values of reconstruction band d_{min}

it is observed that the $RMSE$ improves with increasing d_{min} . However, for high noise levels after a certain value of d_{min} $RMSE$ begins to increase. It has been observed that a value of $d_{min} = 5$ gives a good performance in both low and high noise levels. A value of $d_{min} = 5$ is adopted for the following tests, this value results in the same order of magnitude of $std_{\hat{g}}$. On the other hand, it is worth mentioning that for the same reconstruction band and noise level, the error obtained by applying FSST is slightly lower than the error obtained by FSST2.

3) *Dissipating Energy Flow*: For the DEF calculation, in addition to filtering the electrical power, it is necessary to perform the decomposition of the reactive power flow signals Q , voltage V and voltage angle θ . Fig. 9 shows DEF of different generators calculated from FSST and FSST2 for different levels of added noise. Generator 112 is indicated in blue in Fig. 5, it has been chosen randomly to consider another generator where there is no disturbance. $h = 1$ is the fundamental frequency component of the square signal of the disturbance in generator 79 and $h = 2$ corresponds to the 0.7 Hz mode of disturbance in generator 15. In all cases, generator 79 is identified as the source of component $h = 1$ and generator 15 as source of component $h = 2$. The performance of FSST and FSST2 is very similar in this case.

B. ISO-NE October 3, 2017 Event

Fig. 10 shows the curves identified applying the proposed methodology over multi-channel using STFT, FSST and FSST2, alternatively. Multi-channel TF representations are calculated from the measurements of the active and reactive power flows of the 32 monitored branches, whose data were obtained from [7]. It can be observed that using any of the three TF representations, it is possible to identify the time-variable harmonics of the forced oscillation. In the case of STFT, a mode mixing occurs between the fourth and sixth harmonics. Then, using the identified curves in the TF plane, active power flows P , reactive power flow signals Q , voltage

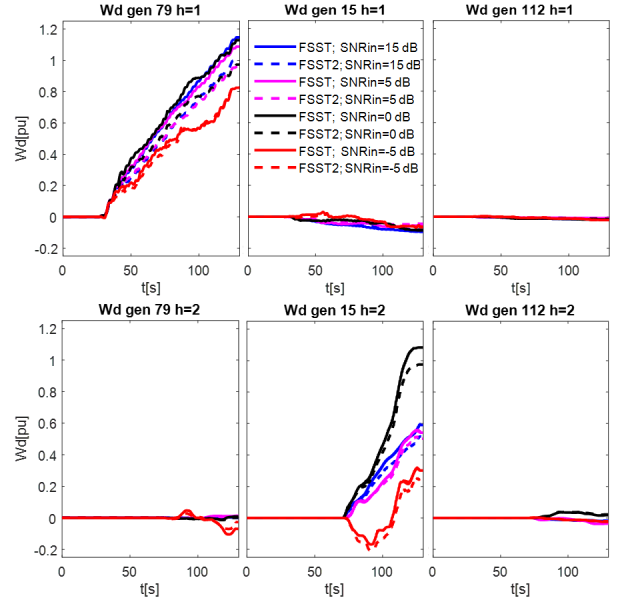


Fig. 9. Dissipating Energy Flow Wd of different generators calculated from FSST and FSST2 for different levels of added noise.

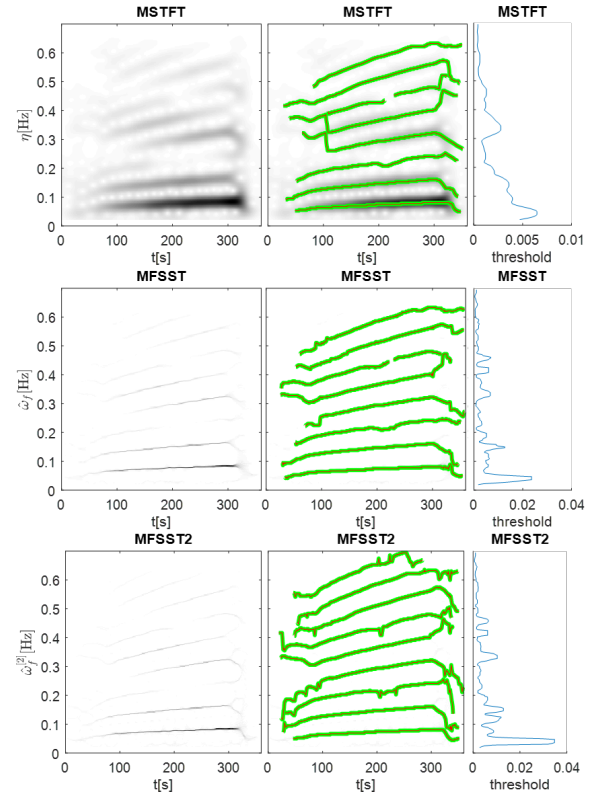


Fig. 10. Application of multi-channel frequency identification on real PMU data from October 3, 2017 event in ISO-NE

V and voltage angle θ can be decomposed, in order to calculate DEF to trace the source of oscillation. The DEF results are similar for any of the three reconstruction alternatives (using STFT, FSST or FSST2) and also similar to those obtained in [13]. For space reasons, these results are not presented in this work. The main difference is that in [13] the oscillatory components were identified by decomposing the most representative signal of the oscillation and in a time

window previously determined where oscillation was clearly present with the naked eye. Using this new approach, multi-channel analysis does not need to take any prior consideration on the signal or the instance where the FO is presence.

C. IEEE-NASPI Oscillation Source Location Contest

The proposed methodology in this paper was applied in the IEEE-NASPI Oscillation Source Location Contest [20]. A total of 13 cases were studied with the following characteristics [21]. Synthetic PMU measurements of bus voltage and branch current phasors from multiple locations of the test system were provided. There was a 30 seconds leading window before the event and 60 seconds time window after that, total 90 seconds of data. White noise was added to the load during simulation to mimic random load fluctuations. Powertech Lab's TSAT software was used for the time-domain simulation. EPRI's PMU Emulator was used to process the simulation results to mimic PMU device performance, a mix of P Class (2-cycle window) and M Class (6-cycle window) PMUs were used. EPRI's Synchrophasor Data Conditioning Tool was used to process the synthetic PMU data to introduce data quality problems. Each data set consisted of four text files for Bus voltage magnitudes, Bus voltage angles, Branch current magnitudes, and Branch current angles. From a participation of 21 teams, our Team reached third place [22].

V. CONCLUSIONS

This paper proposes a systematic methodology for the identification and filtering of non-stationary oscillatory components of FO in power systems based on a multi-channel representation in the time-frequency plane. In particular, a methodology is developed for the definition of a spectrum-dependent threshold to discriminate the presence of FO. In addition, an improved ridge identification algorithm and hard-thresholding signal reconstruction based on a spectrum-dependent threshold is developed. We study the performance on TF approaches: short-time Fourier transform (STFT), STFT-based synchrosqueezing transform (FSST) and second order FSST (FSST2). It is shown that due to the sharper and more concentrated spectrum around ridges, FSST and FSST2 present a clear advantage over STFT regarding the performance of the algorithm for the identification of peak curves, minimizing the mixing of modes. In cases where the oscillatory components of the signal are well separated in frequency and do not have a high frequency modulation, the three TFRs give similar results. On the other hand, for non-stationary oscillations with high frequency modulations, the FSST2 method has the advantage of being able to concentrate the spectrum even for very high frequency modulations. However, available event measurements of power systems FO have shown that very high frequency modulations do not occur normally. Therefore, the use of FSST gives a good compromise relationship between resolution and computational demand. The methodology could be applied with other invertible TFRs such as multisynchrosqueezing transform [23], CWT or CWT-based SST. The effectiveness of the proposed methodology was tested on simulated data, data of the real operation and

also applied successfully in the cases of the IEEE-NASPI OSL Contest 2021 [22].

REFERENCES

- [1] J. Follum and J. W. Pierre, "Detection of periodic forced oscillations in power systems," *IEEE Trans. on Power Syst.*, vol. 31, no. 3, pp. 2423–2433, May 2016.
- [2] J. Follum, J. W. Pierre, and R. Martin, "Simultaneous estimation of electromechanical modes and forced oscillations," *IEEE Trans. on Power Syst.*, vol. 32, no. 5, pp. 3958–3967, Sep 2017.
- [3] N. R. Guideline, "Forced oscillation monitoring & mitigation," North American Reliability Cooperation, Tech. Rep., 09 2017.
- [4] L. Chen, Y. Min, and W. Hu, "An energy-based method for location of power system oscillation source," *IEEE Trans. on Power Syst.*, vol. 28, no. 2, pp. 828–836, May 2013.
- [5] D. Trudnowski, "Available methods, algorithms and tools for oscillation detection and source location," in *2018 IEEE Power Energy Society General Meeting*, Sep 2018.
- [6] S. Maslennikov and E. Litvinov, "Iso new england experience in locating the source of oscillations online," *IEEE Trans. on Power Syst.*, vol. 36, no. 1, pp. 495–503, 2021.
- [7] S. Maslennikov, X. Xu, K. Sun, B. Wang, (April 2018) Test Cases Library of Power System Sustained Oscillations. [Online]. Available: <http://web.eecs.utk.edu/~kaisun/Oscillation/>
- [8] S. Maslennikov, B. Wang, and E. Litvinov, "Dissipating energy flow method for locating the source of sustained oscillations," *Int. J. Elec. Power*, vol. 88, pp. 55 – 62, 2017.
- [9] I. Daubechies, J. Lu, and H.-T. Wu, "Synchrosqueezed wavelet transforms: An empirical mode decomposition-like tool," *Appl. Comput. Harmon. A.*, vol. 30, no. 2, pp. 243 – 261, 2011.
- [10] T. Oberlin, S. Meignen, and V. Perrier, "The fourier-based synchrosqueezing transform," in *2014 IEEE Int. Conference on Acoustics, Speech and Signal Processing (ICASSP)*, May 2014, pp. 315–319.
- [11] T. Oberlin, S. Meignen and V. Perrier, "Second-order synchrosqueezing transform or invertible reassignment? towards ideal time-frequency representations," *IEEE Trans. on Signal Processing*, vol. 63, no. 5, pp. 1335–1344, 2015.
- [12] R. Behera , S. Meignen , T. Oberlin, "Theoretical analysis of the second-order synchrosqueezing transform," *Appl. Comput. Harmon. Anal.*, vol. 45, no. 2, pp. 379–404, 2018.
- [13] P. Gill Estevez, P. Marchi, C. Galarza and M. Elizondo, "Non-stationary power system forced oscillation analysis using synchrosqueezing transform," *IEEE Transactions on Power Systems*, vol. 36, no. 2, pp. 1583–1593, 2021.
- [14] G. Thakur, E. Brevdo, N. S. Fućkar, and H.-T. Wu, "The synchrosqueezing algorithm for time-varying spectral analysis: Robustness properties and new paleoclimate applications," *Signal Processing*, vol. 93, no. 5, pp. 1079 – 1094, 2013.
- [15] N. Laurent and S. Meignen, "A novel time-frequency technique for mode retrieval based on linear chirp approximation," *IEEE Signal Processing Letters*, vol. 27, pp. 935–939, 2020.
- [16] T. G. S. Meignen and T. Oberlin, "Time-frequency ridge analysis based on the reassignment vector," in *2015 23rd European Signal Processing Conference (EUSIPCO)*, 2015, pp. 1486–1490.
- [17] S. Meignen, D. Pham and S. McLaughlin, "On demodulation, ridge detection, and synchrosqueezing for multicomponent signals," *IEEE Transactions on Signal Processing*, vol. 65, no. 8, pp. 2093–2103, 2017.
- [18] D. Pham and S. Meignen, "A novel thresholding technique for the denoising of multicomponent signals," in *2018 IEEE International Conference on Acoustics, Speech and Signal Processing (ICASSP)*, 2018, pp. 4004–4008.
- [19] N. Laurent. (April 2020) STFT, FSST and FSST2 Code. [Online]. Available: <https://github.com/Nils-Laurent/LCR>
- [20] (July 2021) IEEE-NASPI Oscillation Source Location Contest. [Online]. Available: <https://www.naspi.org/node/890>
- [21] (July 2021) Test Cases of IEEE-NASPI Oscillation Source Location Contest. [Online]. Available: <http://web.eecs.utk.edu/~kaisun/Oscillation/2021Contest/>
- [22] (July 2021) IEEE-NASPI Oscillation Source Location Contest Winners. [Online]. Available: <https://www.naspi.org/node/913>
- [23] G. Yu, Z. Wang, and P. Zhao, "Multisynchrosqueezing transform," *IEEE Transactions on Industrial Electronics*, vol. 66, no. 7, pp. 5441–5455, 2019.